Effect of Coil Torsion on Heat Transfer and Pressure Drop Characteristics of Shell and Coil Heat Exchanger

Article *in* Journal of Thermal Science and Engineering Applications · November 2015

DOI: 10.1115/1.4030732

4 authors:

Mohamed Reda Salem
Benha University
4 PUBLICATIONS **4** CITATIONS
SEE PROFILE

K. M. El-Shazly
Benha University
26 PUBLICATIONS **37** CITATIONS
SEE PROFILE

Ramadan Youssef Sakr
Benha University
19 PUBLICATIONS **25** CITATIONS
SEE PROFILE

Ragab Khalil Ali
Benha University
12 PUBLICATIONS **18** CITATIONS
SEE PROFILE

M. R. Salem
Mechanical Engineering Department,
Faculty of Engineering at Shoubra,
Benha University,
108 Shoubra Street,
Cairo 11629, Egypt
e-mail: me_mohamedreda@yahoo.com

K. M. Elshazly
Mechanical Engineering Department,
Faculty of Engineering at Shoubra,
Benha University,
108 Shoubra Street,
Cairo 11629, Egypt
e-mail: drkaramelshazly@yahoo.com

R. Y. Sakr
Mechanical Engineering Department,
Faculty of Engineering at Shoubra,
Benha University,
108 Shoubra Street,
Cairo 11629, Egypt
e-mail: rsakr85@yahoo.com

R. K. Ali
Mechanical Engineering Department,
Faculty of Engineering at Shoubra,
Benha University,
108 Shoubra Street,
Cairo 11629, Egypt
e-mail: ragabkhalil1971@gmail.com

Effect of Coil Torsion on Heat Transfer and Pressure Drop Characteristics of Shell and Coil Heat Exchanger

The present work introduces an experimental study of horizontal shell and coil heat exchangers. Characteristics of the convective heat transfer in this type of heat exchangers and the friction factor for fully developed flow through their helically coiled tube (HCT) were investigated. The majority of previous studies were performed on HCTs with isothermal and isoflux boundary conditions or shell and coil heat exchangers with small ranges of HCT configurations and fluid-operating conditions. Here, five heat exchangers of counterflow configuration were constructed with different HCT torsions (λ) and tested at different mass flow rates and inlet temperatures of both sides of the heat exchangers. In total, 295 test runs were performed from which the HCT-side and shell-side heat transfer coefficients were calculated. Results showed that the average Nusselt numbers of both sides of the heat exchangers and the overall heat transfer coefficient increase by decreasing coil torsion. At lower and higher HCT-side Reynolds number (Re_t), the average increase in the HCT-side average Nusselt number ($\overline{Nu}_t$) is of 108.7% and 58.6%, respectively, when λ decreases from 0.1348 to 0.0442. While, at lower and higher shell-side Reynolds number (Re_{sh}), the average increase in the shell-side average Nusselt number ($\overline{Nu}_{sh}$) is of 173.9% and 69.5%, respectively, when λ decreases from 0.1348 to 0.0442. In addition, a slight increase of 6.4% is obtained in the HCT Fanning friction factor (f_c) at lower Re_t when λ decreases from 0.1348 to 0.0442, and this effect vanishes with increasing Re_t. Furthermore, correlations for $\overline{Nu}_t$, $\overline{Nu}_{sh}$, and f_c are obtained.
[DOI: 10.1115/1.4030732]

Keywords: heat exchanger, helically coiled tube, torsion, friction, experimental

1 Introduction

Helical shape of coiled tubes is one of the enhancement techniques that are widely used as heat exchangers and have applications in various industries: chemical, biological, petrochemical, mechanical, biomedical, and others. This wide use of the HCTs is because they have large heat transfer areas and promote good mixing of the fluids, which enhances the heat transfer coefficients [1,2]. Due to the extensive application of the HCTs in these fields, knowledge about the heat transfer and pressure drop characteristics is very important.

Coil torsion is one of the geometrical parameters that affect the fluid flow in the HCT; it is the ratio of the coil pitch (p_c) to the developed length of one turn (πD_c).

It was shown that the secondary flow patterns, due to the coil curvature, are affected by coil torsion leading to distortions in the patterns from the classical symmetrical shape (of flow without torsion) and skews the velocity profiles in the direction of the torsion [3–7].

There are several studies in the literature concerning the friction losses in HCTs [8–17]. These studies reported that an increase in the flow resistance compared with straight tubes. This is due to the centrifugal force caused by the pipe curvature. Correlations were obtained as a function of Re_t, δ, and Dean number (De). De is a dimensionless group that measures the ratio of the geometric average of inertial and centrifugal forces to the viscous forces, defined according to Eq. (1) in which Re_t is the HCT Reynolds number based on axial flow. Since the secondary flow is induced by centrifugal forces and their interaction primarily with viscous forces, De becomes a general measure of the magnitude of the secondary flow. δ is a dimensionless coil curvature ratio; it is the ratio of the inner diameter of the HCT ($d_{t,i}$) to the mean diameter of the coil curvature (D_c)

$$De = Re_t \delta^{0.5} \tag{1}$$

The effect of coil torsion on pressure drop for fully developed flow in HCTs [18–20] reported that for same δ and De, the effect of increasing λ is seen to reduce the resistance in the tube.

Experimental results for forced convection heat transfer for turbulent flow of water through steam-heated coiled tubes were reported by Rogers and Mayhew [12]. Three coils with δ of 0.0926, 0.075, and 0.05 were used during experiments. They proposed a correlation for Re_t between 10,000 and 100,000. Austen and Soliman [13] studied the effect of λ on heat transfer for the case of uniform wall heat flux. Results showed significant effects of λ on $\overline{Nu}_t$ at low Re_t, though these effects weakened as Re_t increased.

The effect of λ on heat transfer behavior was investigated numerically for uniformly heated HCT by Yang et al. [14] for laminar flow and by Yang and Ebadian [15] for turbulent flow. It was shown that the torsion rotates and distorts the temperature profiles. Overall, $\overline{Nu}_t$ decreased with increasing torsion for $Pr_t < 1$, but it significantly decreased with larger Pr_t.

Xin and Ebadian [21] experimentally studied the effect of Pr_t and geometric parameters on the local and average convective heat transfer characteristics in HCTs. In their studies, experiments with three different fluids, air, water, and ethylene glycol, were

Contributed by the Heat Transfer Division of ASME for publication in the Journal of Thermal Science and Engineering Applications. Manuscript received May 4, 2014; final manuscript received February 11, 2015; published online November 11, 2015. Assoc. Editor: P. K. Das.

carried out on uniformly heated HCT. Empirical correlations were proposed for the fully developed flow ($0.0637 < \lambda < 0.8149$).

Bai et al. [22] experimentally studied the turbulent heat transfer in horizontal HCTs under constant heat flux. They concluded that the local heat transfer coefficient on the outer wall could be three to four times that of the inner wall, and it is observed that $\overline{Nu}_t$ for horizontal HCT is less than that for vertical one for the same conditions. Prabhanjan et al. [18] compared experimentally the heat transfer coefficient for HCT versus straight tube heat exchangers. They found that the HCT had a heat transfer coefficient of 1.16 and 1.43 times larger than for the straight tube heat exchanger for 40 °C and 50 °C, respectively.

Rennie and Raghavan [19,20] performed numerical and experimental studies on a double-pipe helical heat exchanger. Results showed that the overall heat transfer coefficients increase as De increases. However, flow conditions in the annulus had a stronger influence on the overall heat transfer coefficient. Salimpour [23,24] experimentally studied the heat transfer characteristics for laminar flow of oil and water inside HCT counterflow configurations with small spacing between coil turns of 5, 5.4, and 10.7 mm. Empirical correlations were developed to predict the heat transfer coefficients of the both fluids inside the HCT as a function of De, Pr_t, and λ.

Purandare et al. [25] presented a comparative analysis of the different correlations given by the different researchers for helical coil heat exchanger. The analysis showed that, for low Re_t, the graphs of $\overline{Nu}_t$ versus Re_t are steeper than that at high Re_t. In addition, HCTs are efficient in low Re_t.

Salem et al. [26] experimentally investigated the characteristics of convective heat transfer in horizontal shell and coil heat exchangers, in addition to friction factor for fully developed flow through the HCT. Five heat exchangers of counterflow configuration were constructed with different HCT curvature ratios. Results showed that $\overline{Nu}$ of the two sides of the heat exchangers and friction factor through the HCT increased by increasing coil-curvature ratio. Correlations for $\overline{Nu}$ for both heat exchanger sides and the HCT Fanning friction factor as a function of Re, Pr, and δ were developed.

The aforementioned literature survey indicates that the majority of studies performed on HCT with isothermal and isoflux boundary conditions or shell and coil heat exchangers with small ranges of HCT configurations and fluid operating conditions. So, the present study aims to investigate experimentally the effect coil torsion on characteristics of convective heat transfer in horizontal shell and coil heat exchangers with same curvature ratio over a wide range of fluid-operating conditions. Present measurements were utilized to introduce experimental correlations for the average Nusselt numbers and the HCT Fanning friction factor as a function of Reynolds number, coil torsion, and Prandtl number.

2 Experimental Setup

The experimental facility employed in the present investigation consists of heating and cooling units, shell and coil heat exchanger, pumps, measuring devices, valves, and the connecting pipes. As illustrated in Fig. 1, each circuit contains bypass line and ball valve to control the mass flow rate directed to the heat exchanger. Two identical flow meters (1.7–18 l/min) were used to measure the volume flow rates directed to the test section. Twenty-eight *k*-type thermocouples of 0.1 mm diameter were installed within each test section to measure the temperatures. Four thermocouples were inserted into the flow streams, at approximately 60 mm from the heat exchanger ports, to measure the inlet and exit temperatures of the shell and HCT fluids.

Figure 2 represents a photograph for the present setup. Two cylindrical containers of 50 l made of stainless steel (2 mm wall thickness) were employed for hot and cold fluid tanks. Each tank was installed inside 2 mm thick galvanized steel tanks with 20 mm gap, which was injected by Polyurethane spray foam insulation to minimize the heat loss or gain. An electric heater of 6 kW rated power was fixed horizontally at the bottom of the heating tank to heat the water to the required temperature. The heat was removed from the water in the cooling tank by two cooling units of 10.5 kW cooling capacity. Sometimes, the two cooling units operate in series, and in other times, in parallel manner to prevent thermal overloads. The operations of the electric heater and the cooler were based on pre-adjusted digital thermostats, which were used to keep constant temperatures of the liquids directed to the heat exchanger, whether for the HCT-side or the shell-side.

Twenty thermocouples were used to measure the HCT wall surface temperatures. They were mounted at ten equally distanced (441.5 mm) positions on the HCT surface, with installing two thermocouples at each position on the outer and inner diameters of the coil. To achieve higher accuracy in calculation of flow rate, four thermocouples were installed at inlet and exit of flow meters to record the flow temperature. All thermocouples were connected to a digital thermometer indicator with resolution of 0.1 °C to display the thermocouples outputs. A digital differential pressure transducer was employed for measuring the pressure drop of water across the HCT. Two identical 1.5 hp rated power centrifugal pumps were installed to circulate the hot and cold water. Flexible nylon and polyvinyl chloride (PVC) tubes were used for all connections.

Five configurations of shell and coil heat exchanger were constructed with different HCT torsions. The dimensions of the copper tube used in each coil are 4415 mm lengths, 9.52 mm outer diameter, and 8.3 mm inner diameter. The mean diameter of the five coils is 140.5 mm, which resulted in a coil curvature ratio of 0.0591 and number of coil turns of 10. The length of the shells (L_{sh}) and their internal diameters ($D_{sh,i}$) were calculated to achieve same hydraulic diameter of the shell side ($D_{sh,h}$) for all heat exchangers. The characteristic dimensions of the different configurations are revealed in Table 1. A photograph and schematic diagram of the shell and coil heat exchanger are shown in Fig. 3.

The shell of the heat exchangers was made of mild steel (2 mm wall thickness) and was formed as cylindrical shape. Two nipples, of the same material and 4 mm wall thickness, were welded on both ends of the shell. Ten holes of 1 mm diameter were made in the shell wall to pass the thermocouples to their positions on the HCT surface. The holes were drilled directly facing the positions of the thermocouples to provide the smallest length of the thermocouples in the shell to minimize their effects on the shell flow. The outer surface of the shell was thermally isolated with thick insulation using a layer of each ceramic fiber, asbestos rope, and glass wool. Finally, all equipments were assembled: the shell and coil heat exchanger, heating and cooling units, pumps, ball valves, connecting lines, and the measuring devices.

3 Experimental Procedures and Data Reduction

The first step in collecting data from the system was to fill the heating and cooling tanks with water from the local water supply. Then, the heater, the cooling units, and the pumps were turned on. Inlet temperatures of the water in both sides were adjusted by regulating the temperatures of the heating and cooling tanks through their thermostats. The flow rates were adjusted through the flow meters and the installed valves, which were regulated to obtain the required flow rates in the primary lines and the remainder is bypassed to the tanks. The range of the operating conditions is given in Table 2.

During the operation, the steady-state condition is conducted when the maximum variation of 0.5 °C for each thermocouple reading within 20 min. It should be noted that for heat transfer calculations, the fluid properties of the shell and HCT sides were calculated at the bulk temperatures, $T_{sh,m}$ and $T_{t,m}$, respectively. While for pressure drop calculations, the HCT water properties were calculated at the film temperature, T_f, as recommended by Schmidt [27]. The bulk and film temperatures are calculated as follows:

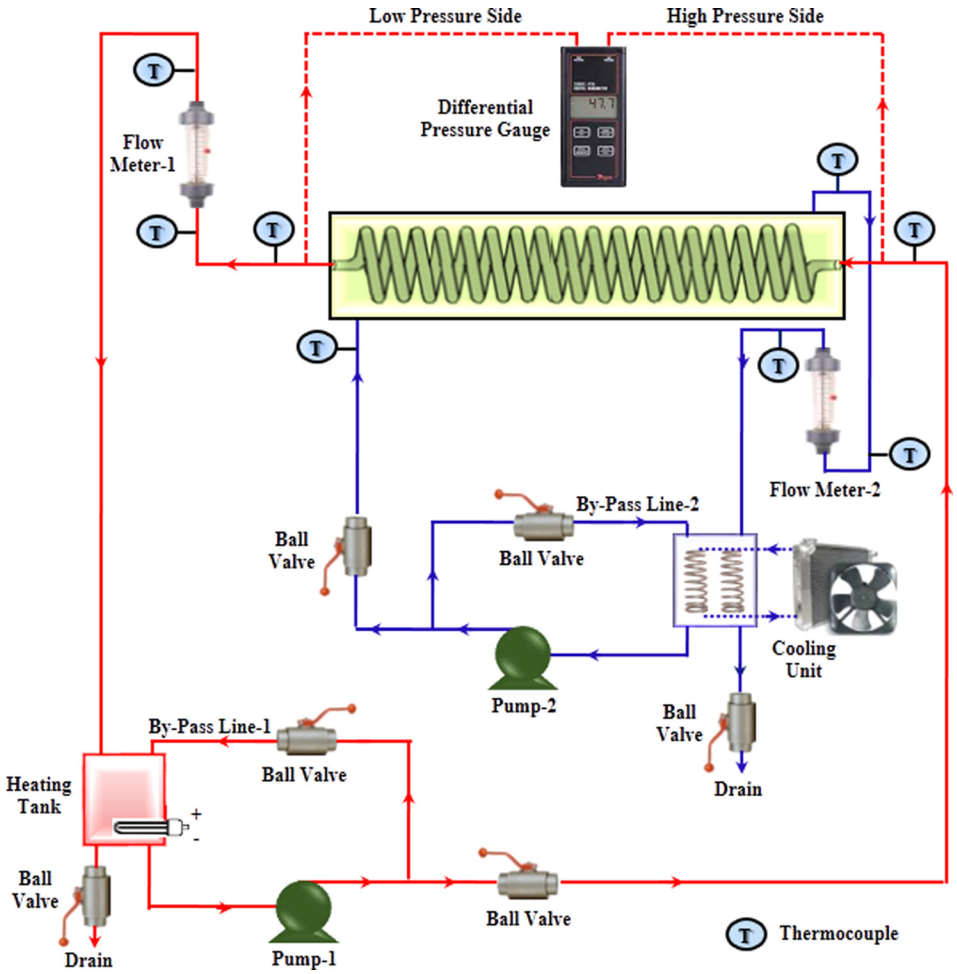

Fig. 1 Schematic diagram of the experimental apparatus

$$T_{\mathrm{sh,m}} = \left(T_{\mathrm{sh,i}} + T_{\mathrm{sh,o}}\right)/2 \tag{2}$$

$$T_{\mathrm{t,m}} = \left(T_{\mathrm{t,i}} + T_{\mathrm{t,o}}\right)/2 \tag{3}$$

$$\bar{T}_{\mathrm{t,s}} = \frac{\sum T_{\mathrm{t,s}}}{20} \tag{4}$$

$$T_{\mathrm{f}} = \left(T_{\mathrm{t,m}} + \bar{T}_{\mathrm{t,s}}\right)/2 \tag{5}$$

The inner surface temperature of the HCT wall was taken equal to outer surface due to very low conduction resistance of the tube wall. The water thermophysical properties were evaluated from Ralph [28].

Fig. 2 Photograph for the experimental apparatus

The measurements of the flow rates and inlet and outlet temperatures of both streams of the heat exchanger were used to calculate heat transfer rates on the HCT and shell sides (Q_{t} and Q_{sh}) as

$$Q_{\mathrm{t}} = \dot{m}_{\mathrm{t}}\mathrm{Cp}_{\mathrm{t}}\left(T_{\mathrm{t,i}} - T_{\mathrm{t,o}}\right) \tag{6}$$

$$Q_{\mathrm{sh}} = \dot{m}_{\mathrm{sh}}\mathrm{Cp}_{\mathrm{sh}}\left(T_{\mathrm{sh,o}} - T_{\mathrm{sh,i}}\right) \tag{7}$$

Without heat gain or loss from the heat exchanger, there is an energy balance between the two streams ($Q_{\mathrm{t}} = Q_{\mathrm{sh}}$). In the real experiments, there would always be some discrepancy between the two heat transfer rates. Therefore, the arithmetical average of the two, Q_{ave}, can be used as the heat load of the exchanger. For all experimental tests, the heating and cooling loads calculated from the hot and cold sides did not differ by more than $\pm 1.9\%$.

$$Q_{\mathrm{ave}} = \frac{|Q_{\mathrm{t}}| + |Q_{\mathrm{sh}}|}{2} \tag{8}$$

Table 1 Characteristic dimensions of the used shell and coil heat exchangers

HCT no.	p_{c} (mm)	λ	L_{sh} (mm)	$D_{\mathrm{sh,i}}$ (mm)	$D_{\mathrm{sh,h}}$ (mm)
1	19.52	0.0442	305	303	205.1
2	29.52	0.0669	405	284	
3	39.52	0.0895	505	271	
4	49.52	0.1122	605	262	
5	59.52	0.1348	705	255	

The heat load of the heat exchanger, Q_{ave}, was used to calculate the average heat transfer coefficient for the HCT side fluid, $\bar{h}_t$, and then the average Nusselt number for the HCT side fluid, $\overline{Nu}_t$, as follows:

$$Q_{ave} = \bar{h}_t A_{t,i}\left(T_{t,m} - \bar{T}_{t,s}\right) \tag{9}$$

$$Nu_t = \frac{\bar{h}_t d_{t,i}}{k_t} \tag{10}$$

The overall thermal conductance was calculated from the temperature data and flow rates using Eq. (11) as follows:

$$U_o A_{t,o} = \frac{Q_{ave}}{\Delta T_{L.M}} \tag{11}$$

$$\Delta T_{L.M} = \frac{\left(T_{t,i} - T_{sh,o}\right) - \left(T_{t,o} - T_{sh,i}\right)}{\ln\left[\frac{T_{t,i} - T_{sh,o}}{T_{t,o} - T_{sh,i}}\right]} \tag{12}$$

Neglecting the thermal resistances of the tube wall and fouling, the overall thermal conductance can be expressed in terms of convection thermal resistances. The average heat transfer coefficient for the shell-side fluid, $\bar{h}_{sh}$, and then the average Nusselt number for the shell-side fluid, $\overline{Nu}_{sh}$, can be obtained as follows:

$$\frac{1}{U_o A_{t,o}} = \frac{1}{\bar{h}_{sh} A_{t,o}} + \frac{1}{\bar{h}_t A_{t,i}} \tag{13}$$

$$\overline{Nu}_{sh} = \frac{\bar{h}_{sh} D_{sh,h}}{k_{sh}} \tag{14}$$

The more general definition of the hydraulic diameter of the shell side, $D_{sh,h}$, described by Shah and Sekulic [29] was used in the present work

$$D_{sh,h} = \frac{4V_f}{A_{f.c}} = \frac{4\left(V_{sh,i} - V_{t,o}\right)}{A_{f.c}} = \frac{D_{sh,i}^2 L_{sh} - d_{t,o}^2 L_t}{D_{sh,i} L_{sh} + d_{t,o} L_t} \tag{15}$$

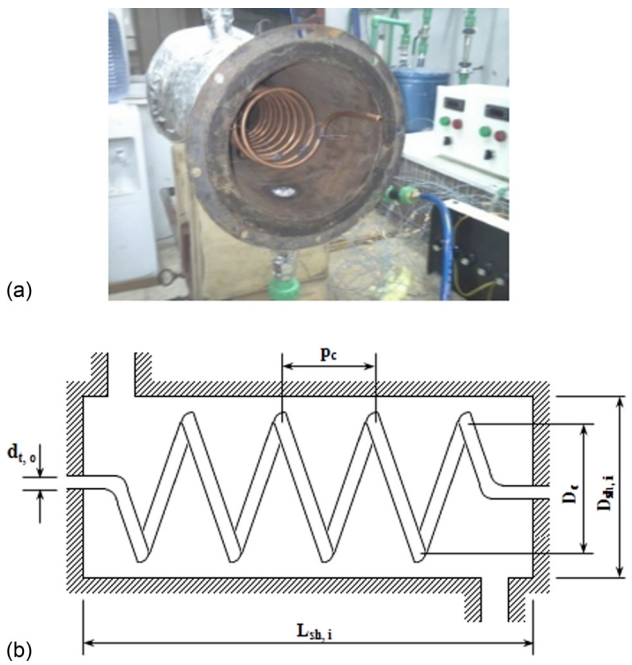

Fig. 3 A photograph and schematic layout of the test section (*a*) photograph of the test section (shell and coil heat exchanger and (*b*) schematic diagram of the shell and coil heat exchanger

HCT and shell Reynolds number can be written as follows:

$$Re_t = \frac{4\dot{m}_t}{\pi d_{t,i}\mu_t} \tag{16}$$

$$Re_{sh} = \frac{4\dot{m}_{sh}}{\pi D_{sh,h}\mu_{sh}} \tag{17}$$

The Fanning friction factor for the fluid in circulation inside the HCT, f_c, was calculated with the following equation:

$$f_c = \frac{\Delta P_c d_{t,i}}{2L_t \rho_t u^2} = \frac{\Delta P_c \pi^2 \rho_t d_{t,i}^5}{32 L_t \dot{m}_t^2} \tag{18}$$

Daily and Harleman [30] reported that the developed region in HCTs may be along a distance equal to 50 diameters of the HCT. Also, Nigam et al. [31] presented that the fully developed region in HCTs is formed after a distance equal to 30 diameters of the HCT. These values represent 5.64–9.4% of the total length of the HCTs used in the present study, which can be neglected and the fully developed profiles are confirmed.

4 Uncertainty Analyses

In general, the accuracy of the experimental results depends on the accuracy of the individual measuring instruments and techniques. It should be noted that according to the manufacturer, uncertainty (ω) in the HCT outer and inner diameters is ± 0.01 mm, which can be neglected. The uncertainty in the measured coil and shell dimensions was assumed to be ± 0.5 mm; this was guessed quantity from meter scale. In addition, the uncertainty applied to the thermal properties of water was assumed to be $\pm 0.1\%$. The uncertainty is calculated based upon the root sum square combination of the effects of each of the individual inputs as introduced by Kline and McClintock [32]. For all experimental runs, the uncertainty in Re_t and Re_{sh} was $\pm 1.7\%$. Also, the average uncertainty was $\pm 4.9\%$ in $\overline{Nu}_t$, $\pm 2.6\%$ in $\overline{Nu}_{sh}$, $\pm 2.2\%$ in U_o, and $\pm 3.7\%$ in f_c.

5 Results and Discussion

First, the experimental apparatus and procedures were validated by comparing the results of $\overline{Nu}_t$ for water flowing through the HCT with $\overline{Nu}_t$ reported from literature. From the literature review, it is obvious that there is lack in the correlations required to calculate the heat transfer coefficient for applied shell and coil heat exchangers. On the contrary, there are a number of correlations in the literature for the $\overline{Nu}_t$ for water flowing through the HCT with isoflux and isothermal wall boundary conditions. Here, the present experimental data for $\overline{Nu}_t$ was validated with the experimental data obtained by Rogers and Mayhew [12], and Xin and Ebadian [21]. In addition, another comparison of the experimental data for HCT Fanning friction factor with the results of White [33] and Prasad et al. [10] was performed. The results of these comparisons are shown in Fig. 4. From this figure, it can be seen that the experimental results for both heat transfer and friction factor calculations are in good agreement with previous studies.

5.1 Heat Transfer Results. A series of 295 experiments was carried out on five heat exchangers shown in Table 1, which were constructed with different coil torsions. First, the operating conditions are hold constant in the shell side at $T_{sh,i} = 20\,^{\circ}C$ and $\dot{V}_{sh} = 6.018$ l/min, while the HCT operating conditions are varied according to Table 2. Figure 5 illustrates $\overline{Nu}_t$ versus HCT Reynolds number at $T_{t,i} = 55\,^{\circ}C$ for $0.0442 \le \lambda \le 0.1348$ as a sample of the results.

From Fig. 5, it is obvious that decreasing coil torsion increases $\overline{Nu}_t$ even at same Re_t and $T_{t,i}$. At lower and higher Re_t, the average increase in $\overline{Nu}_t$ is of 108.7% and 58.6%, respectively, when λ decreases from 0.1348 to 0.0442. This can be attributed to the increase in rotational force as a result of increasing the coil torsion which diminishes the secondary flow that established by the

Table 2 Range of fluids operating conditions

HCT-side	
HCT-side water flow rate (l/min)	$1.7 - 11.158$ ($6511 \leq Re_t \leq 62092$)
HCT-side inlet temperature (°C)	45, 55, 65 ($2.86 \leq Pr_t \leq 4.39$)
Shell-side water flow rate (l/min)	6.018
Shell-side inlet temperature (°C)	20
Shell-side	
Shell-side water flow rate (l/min)	$1.7-11.158$ ($180 \leq Re_{sh} \leq 1383$)
Shell-side inlet temperature (°C)	15, 20, 25 ($5.36 \leq Pr_{sh} \leq 7.52$)
HCT-side water flow rate (l/min)	6.018
side inlet temperature (°C)	55

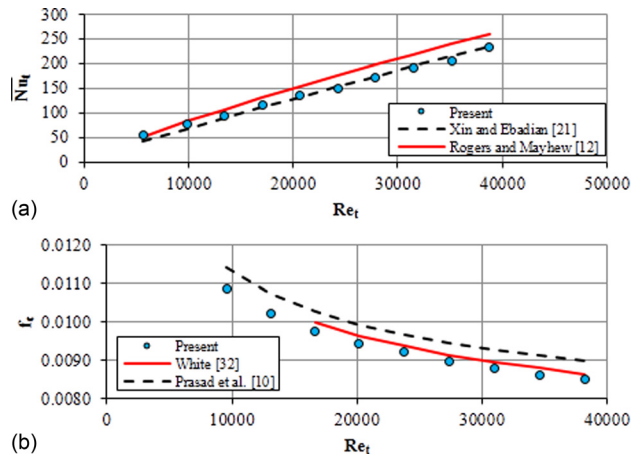

Fig. 4 Validation of the experimental data for HCT ($\lambda = 0.0895$)

centrifugal effect. Also, it is clear that increasing Re_t increases $\overline{Nu}_t$ at the same coil torsion. This can be returned to the effective secondary flow due to centrifugal force, which increases at higher Reynolds number.

The influence of HCT fluid inlet temperature on the thermal performance for these five heat exchanger configurations ($0.0442 \leq \lambda \leq 0.1348$) is studied. A sample of the results is illustrated in Fig. 6 for $\lambda = 0.0895$.

It can be seen from Fig. 6 that as the inlet temperature of the HCT fluid flow increases, $\overline{Nu}_t$ decreases at the same Reynolds number. This can be attributed to the decrease in Prandtl number with increasing the temperature of the fluid.

The thermal performance of the shell side is introduced for $180 \leq Re_{sh} \leq 1383$, $5.36 \leq Pr_{sh} \leq 7.52$, and $0.0442 \leq \lambda \leq 0.1348$. The inlet temperature and flow rate for HCT fluid remains constant at 55°C and 6.018l/min, respectively. Figure 7 shows the shell-average Nusselt number versus shell-side Reynolds number at $T_{sh,i} = 20$°C as a sample of the results.

From Fig. 7, it is obvious that decreasing coil torsion increases $\overline{Nu}_{sh}$ even at same Re_{sh} and $T_{sh,i}$. At lower and higher shell-side Reynolds number, the average increase in $\overline{Nu}_{sh}$ is of 173.9% and 69.5%, respectively, when the coil torsion decreases from 0.1348

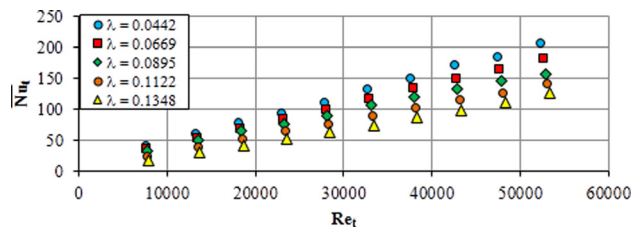

Fig. 5 Variation of HCT average Nusselt number with HCT-side Reynolds number at different coil torsions ($T_{t,i} = 55$ °C)

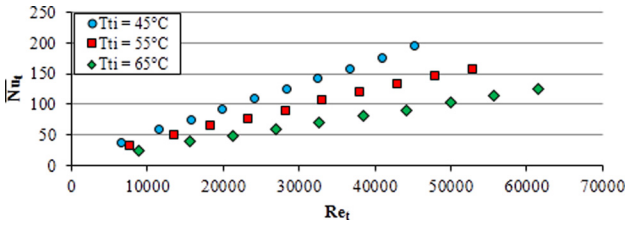

Fig. 6 Variation of HCT average Nusselt number with HCT-side Reynolds number at different HCT inlet temperatures ($\lambda = 0.0895$)

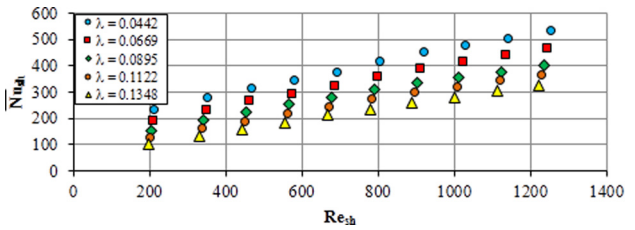

Fig. 7 Variation of shell-average Nusselt number with shell-side Reynolds number at different HCT torsions ($T_{sh,i} = 20$ °C)

to 0.0442. This can be returned to decreasing coil torsion increases the flow impingement on the coil turns and the turbulence level around the outer coil surface due to the decrease in the inclination angle of coil turns associated with the decrease in coil torsion. Also, it is clear that increasing Re_{sh} increases $\overline{Nu}_{sh}$ at the same λ and $T_{sh,i}$. This can be attributed to increasing the fluctuations and fluid layers mixing around the coil turns by increasing Re_{sh}.

The influence of shell inlet temperature on the thermal performance of the heat exchanger is studied for $0.0442 \leq \lambda \leq 0.1348$. The experimental runs were performed for shell inlet fluid temperature at $T_{sh,i} = 15, 20,$ and 25 °C corresponding to $5.36 \leq Pr_{sh} \leq 7.52$. A sample of the results is illustrated in Fig. 8 for $\lambda = 0.0895$.

It is clear from Fig. 9 that as the inlet temperature of the shell-fluid flow increases, $\overline{Nu}_{sh}$ decreases at the same Reynolds number. This can be attributed to the decrease in Prandtl number by increasing the temperature of the fluid.

5.2 Pressure Drop Results. Experimental runs were carried out to study the effects of coil torsion and HCT fluid inlet temperature on the friction factor inside HCT. The mass flow rate is varied from 1.7 to 11.158l/min and coil inlet fluid temperature of $T_{t,i} = 45, 55,$ and 65 °C. The corresponding dimensionless parameters are $6355 \leq Re_t \leq 60234$ and $0.0442 \leq \lambda \leq 0.1348$. Figure 8 presents the effect of coil torsion at $T_{t,i} = 55$ °C as a sample of the results.

From Fig. 8, it is clear that decreasing the coil torsion leads to slight increase in f_c at the same Re_t and $T_{t,i}$. The average increase in HCT Fanning friction factor is of 6.4% obtained at lower Reynolds number when λ decreases from 0.1348 to 0.0442, and this

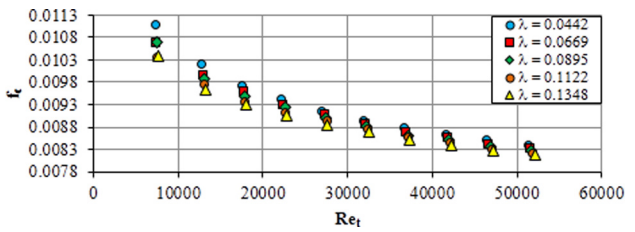

Fig. 8 Variation of HCT Fanning friction factor with HCT-side Reynolds number at different HCT torsions ($T_{t,i} = 55$ °C)

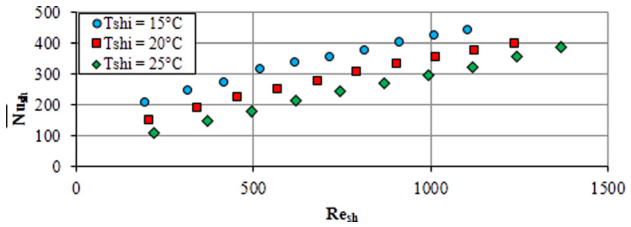

Fig. 9 Shell Nusselt number versus shell Reynolds number at different shell inlet temperatures ($\lambda = 0.0895$)

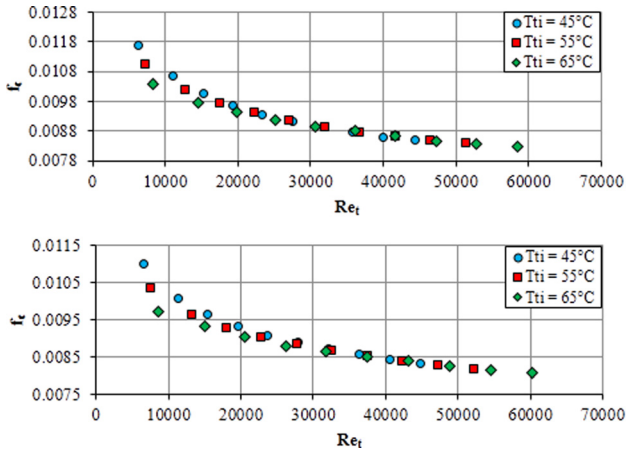

Fig. 10 Effect of HCT-side inlet temperature on the HCT Fanning friction factor; (*a*) $\lambda = 0.0442$ and (*b*) $\lambda = 0.1348$

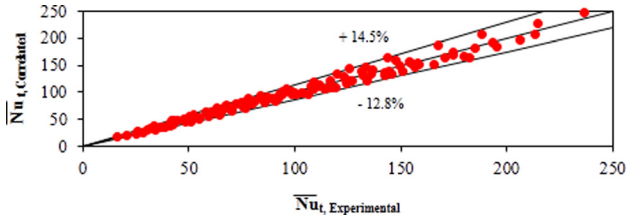

Fig. 11 Comparison of experimental values for HCT average Nusselt number with that correlated by Eq. (19)

effect diminishes with increasing HCT Reynolds number. This can be attributed to the increase in the centrifugal force and consequently vortices formation as a result of decreasing the torsion or rotational effect. Besides, the friction factor decreases as Re_t increases. This can be due to decreasing the viscous boundary layer thickness with increasing Re_t.

Figure 10 shows the effect of HCT fluid inlet temperature on the Fanning friction factor at $\lambda = 0.0442$ and 0.1348. It is clear that the effect of $T_{t,i}$ on f_c is nearly insignificant especially at higher Re_t. This may be returned to the low effect of viscous force compared with the higher centrifugal force, which is the dominant at HCT Reynolds number.

6 Correlations for Average Nusselt Numbers and Fanning Friction Factor

Using the present experimental data, correlations were developed to predict the average Nusselt number of both sides of shell and coil heat exchanger and the Fanning friction factor inside the HCT.

The HCT average Nusselt number is correlated as a function of HCT Reynolds and Prandtl numbers and coil torsion

$$\overline{Nu}_t = 0.000183\,Re_t^{0.9206}\,Pr_t^{2.0934}\,\lambda^{-0.4111} \tag{19}$$

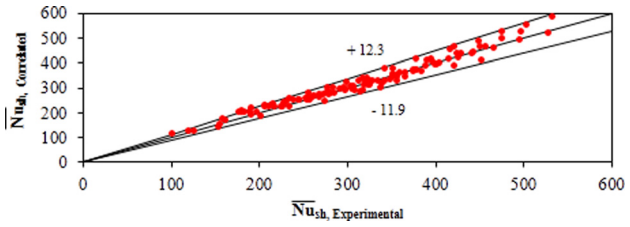

Fig. 12 Comparison of experimental values for shell average Nusselt number with that correlated by Eq. (20)

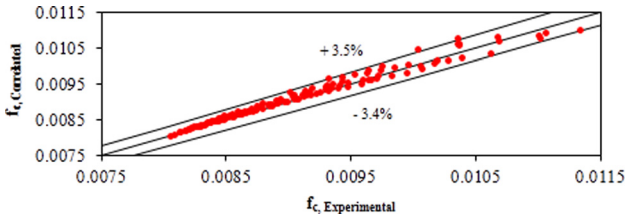

Fig. 13 Comparison of experimental values for coiled tube-Fanning friction factor with that correlated by Eq. (21)

Equation (19) is applicable for $6511 \le Re_t \le 62,092$, $2.86 \le Pr_t \le 4.39$, $1583 \le De \le 15,095$, and $0.0442 \le \lambda \le 0.1348$ with maximum deviation of 14.5%.

From the test runs that were performed for the shell side, a correlation to estimate $\overline{Nu}_{sh}$ was obtained as follows:

$$\overline{Nu}_{sh} = 0.17134\,Re_{sh}^{0.5009}\,Pr_{sh}^{1.4573}\,\lambda^{-0.5919} \tag{20}$$

Equation (20) is applicable for $180 \le Re_{sh} \le 1383$, $5.36 \le Pr_{sh} \le 7.52$, and $0.0442 \le \lambda \le 0.1348$ with maximum deviation of 12.3%.

Additionally, a correlation for Fanning friction factor in the HCT was obtained within $6355 \le Re_t \le 60,234$, $1545 \le De \le 14,643$, and $0.0442 \le \lambda \le 0.1348$ with maximum deviation 3.5%.

$$f_c = 0.03249\,Re_t^{-0.1322}\,\lambda^{-0.0266} \tag{21}$$

From these figures, it is evident that the proposed correlations are in good agreement with the present experimental data (Fig. 11–13).

7 Conclusions

The present work was carried out to investigate the heat transfer characteristics in shell and coil heat exchanger, in addition to the pressure drop inside the HCTs. The investigated ranges are $6511 \le Re_t \le 62,092$, $2.86 \le Pr_t \le 4.39$, $15,095 \le De \le 15,095$, $180 \le Re_{sh} \le 1383$, $5.36 \le Pr_{sh} \le 7.52$, and $0.0442 \le \lambda \le 0.1348$. From the study, it could be concluded that:

- For same operating conditions, the coil torsion has a significant effect on the heat transfer. According to the experimental data, reducing the coil torsion leads to augmenting the average Nusselt numbers of both sides of the heat exchangers. This is because rapid developments of secondary flow enhance heat transfer.
  - At lower and higher HCT Reynolds number, the average increase in $\overline{Nu}_t$ is of 108.7% and 58.6%, respectively, when λ decreases from 0.1348 to 0.0442.
  - At lower and higher shell Reynolds numbers, the average increase in $\overline{Nu}_{sh}$ is of 173.9% and 69.5%, respectively, when λ decreases from 0.1348 to 0.0442.
- For all HCT geometric variables, the operating conditions of the two sides of shell and coil heat exchangers affect directly on their thermal performance. The heat transfer rate goes up

as the mass flow rate increases and as the fluid inlet temperature decreases. This is because rapid developments of secondary flow, turbulence level and increasing Prandtl number enhance heat transfer.

- The HCT Fanning friction factor slightly increases with decreasing coil torsion. The average increase in f_c is 6.4% obtained at lower Re_t when λ decreases from 0.1348 to 0.0442. The influence of coil torsion on f_c vanishes with increasing Re_t.
- Correlations for the average Nusselt numbers of the two sides of shell and coil heat exchanger and the HCT Fanning friction factor were obtained as a function of the investigated parameters.

Nomenclature

A = area, m^2
C_p = specific heat, $J/kg\,^\circ C$
d = diameter, m
D = diameter, m
De = Dean number, Re $\delta^{0.5}$
f = fanning friction factor
k = thermal conductivity, $W/m\cdot^\circ C$
L = length, m
$\dot{m}$ = mass flow rate, kg/s
N = number of turns of the helically coiled tube
$\overline{Nu}$ = average Nusselt number
p = pitch of helically coiled tube, m
P = pressure, Pa
Pr = Prandtl number
Q = heat transfer rate, W
Re = Reynolds number
S = spacing of helically coiled tube, m
T = temperature, °C
u = mean axial velocity, m/s
U = overall heat transfer coefficient, $W/m^2\cdot^\circ C$
V = volume, m^3

Greek Symbols

δ = dimensionless coil curvature ratio, $d_{t,i}/D_c$
λ = dimensionless pitch ratio (coil torsion) $p_c/\pi D_c$
μ = dynamic viscosity, kg/ms
π = Pi ≡ a mathematical constant ≅ 3.1416
ρ = density, kg/m^3
ω = uncertainty

Subscripts and Superscripts

ave = average
c = coil/contact
f = film/fluid/core flow
h = hydraulic
i = inner/inlet/internal
LM = logarithmic mean
m = mean
o = out/outer
s = surface
S = straight tube
sh = shell
t = tube

Abbreviations

HCT = helically coiled tube
PVC = polyvinyl chloride

References

[1] Zhao, Z., Wang, X., Che, D., and Cao, Z., 2011, "Numerical Studies on Flow and Heat Transfer in Membrane Helical-Coil Heat Exchanger and Membrane Serpentine-Tube Heat Exchanger," Int. Commun. Heat Mass Transfer, **38**(9), pp. 1189–1194.
[2] Pimenta, T. A., and Campos, J. B. L. M., 2012, "Friction Losses of Newtonian and Non-Newtonian Fluids Flowing in Laminar Regime in a Helical Coil," Exp. Therm. Fluid Sci., **36**, pp. 194–204.
[3] Kao, H. C., 1987, "Torsion Effect on Fully Developed Flow in a Helical Pipe," J. Fluid Mech., **184**, pp. 335–356.
[4] Liu, S., and Masliyah, J. H., 1994, "Developing Convective Heat Transfer in Helical Pipes With Finite Pitch," Int. J. Heat Fluid Flow, **15**(1), pp. 66–74.
[5] Hüttl, T. J., and Friedrich, R., 2001, "Direct Numerical Simulation of Turbulent Flows in Curved and Helically Coiled Pipes," Comput. Fluids, **30**(5), pp. 591–605.
[6] Gammack, D., and Hydon, P. E., 2001, "Flow in Pipes With Non-Uniform Curvature and Torsion," J. Fluid Mech., **433**, pp. 357–382.
[7] Masud, M. A., Rabiul Islam, Md., Rasel Sheikh, Md., and Mahmud Alam, Md., 2010, "Stable Solution Zone for Fluid Flow Through Curved Pipe With Circular Cross-Section," J. Nav. Archit. Mar. Eng., **7**(1), pp. 19–26.
[8] Austin, L. R., and Seader, J. D., 1973, "Fully Developed Viscous Flow in Coiled Circular Pipes," AIChE J., **19**(1), pp. 85–94.
[9] Mishra, P., and Gupta, N., 1979, "Momentum Transfer in Curved Pipes. 1-Newtonian Fluids," Ind. Eng. Chem. Process Des. Dev., **18**(1), pp. 130–137.
[10] Prasad, B. V. S. S. S., Das, D. H., and Prabhakar, A. K., 1989, "Pressure Drop, Heat Transfer and performance of a Helical Coil Tubular Exchanger," J. Heat Recovery Comb. Heat Power, **9**(3), pp. 249–256.
[11] Ali, S., "Pressure Drop Correlations for Flow Through Regular Helical Coil Tubes," Fluid Dyn. Res., **28**(4), pp. 295–310.
[12] Rogers, G. F. C., and Mayhew, Y. R., 1964, "Heat Transfer and Pressure Loss in Helically Coiled Tubes With Turbulent Flow," Int. Heat Mass Transfer, **7**(11), pp. 1207–1216.
[13] Austen, D. S., and Soliman, H. M., 1988, "Laminar Flow and Heat Transfer in Helically Coiled Tubes With Substantial Pitch," Exp. Therm. Fluid Sci., **1**(2), pp. 183–194.
[14] Yang, G., Dong, F., and Ebadian, M. A., 1995, "Laminar Forced Convection in a Helicoidal Pipe With Finite Pitch," Int. J. Heat Mass Transfer, **38**(5), pp. 853–862.
[15] Yang, G., and Ebadian, M. A., 1996, "Turbulent Forced Convection in a Helicoidal Pipe With Substantial Pitch," Int. J. Heat Mass Transfer, **39**(10), pp. 2015–2022.
[16] Cengiz, Y., Yasar, B., and Dursun, P., 1997, "Heat Transfer and Pressure Drops in a Heat Exchanger With a Helical Pipe Containing Inside Springs," Energy Convers. Manage., **38**(6), pp. 619–624.
[17] Rahul, S., Gupta, S. K., and Subbarao, P. M. V., 1997, "An Experimental Study for Estimating Heat Transfer Coefficient From Coiled Tube Surfaces in Cross-Flow of Air," Third ISHMT-ASME Heat and Mass Transfer Conference and Fourth National Heat and Mass Transfer Conference, IIT Kanpur, Dec. 31, pp. 381–385.
[18] Prabhanjan, D. G., Raghavan, G. S. V., and Rennie, T. J., 2002, "Comparison of Heat Transfer Rates Between a Straight Tube Heat Exchanger and a Helically Coiled Heat Exchanger," Int. Commun. Heat Mass Transfer, **29**(2), pp. 185–191.
[19] Rennie, T. J., and Raghavan, V. G. S., 2005, "Experimental Studies of a Double-Pipe Helical Heat Exchanger," Exp. Therm. Fluid Sci., **29**(8), pp. 919–924.
[20] Rennie, T. J., and Raghavan, G. S. V., 2006, "Numerical Studies of a Double-Pipe Helical Heat Exchanger," Appl. Therm. Eng., **26**(11–12), pp. 1266–1273.
[21] Xin, R. C., and Ebadian, M. A., 1997, "The Effects of Prandtl Numbers on Local and Average Convective Heat Transfer Characteristic in Helical Pipes," ASME J. Heat Transfer, **119**(3), pp. 467–473.
[22] Bai, B., Guo, L., Feng, Z., and Chen, X., 1999, "Turbulent Heat Transfer in a Horizontally Coiled Tube," Heat Transfer-Asian Res., **28**(5), pp. 395–403.
[23] Salimpour, M. R., 2008, "Heat Transfer Characteristics of a Temperature-Dependent-Property Fluid in Shell and Coiled Tube Heat Exchangers," Int. Commun. Heat Mass Transfer, **35**(9), pp. 1190–1195.
[24] Salimpour, M. R., 2009, "Heat Transfer Coefficients of Shell and Coiled Tube Heat Exchangers," Exp. Therm. Fluid Sci., **33**(2), pp. 203–207.
[25] Purandare, P. S., Lele, M. M., and Gupta, R., 2012, "Parametric Analysis of Helical Coil Heat Exchanger," Int. J. Eng. Res. Technol., **1**(8), pp. 1–5.
[26] Salem, M. R., Elshazly, K. M., Sakr, R. Y., and Ali, R. K., 2014, "Experimental Investigation of Coil Curvature Effect on Heat Transfer and Pressure Drop Characteristics of Shell and Coil Heat Exchanger," ASME J. Therm. Sci. Eng. Appl., **7**(1), p. 011005.
[27] Schmidt, E. F., 1967, "Heat Transfer and Pressure Loss in Spiral Tubes," Chem. Ing. Tech., **39**(13), pp. 781–789.
[28] Ralph, R., 2001, *Thermal Design of Electronic Equipment* (Electronics Handbook Series), CRC Press, Boca Raton, FL.
[29] Shah, R. K., and Sekulic, D. P., 2003, *Fundamentals of Heat Exchanger Design*, Wiley, New York.
[30] Daily, J. W., and Harleman, D. R., 1966, *Fluid Dynamics*, Addison-Wesley, Don Mills, ON, Canada.
[31] Nigam, K. D. P., Agarwal, S., and Srivastava, V. K., 2001, "Laminar Convection of Non-Newtonian Fluids in the Thermal Entrance Region of Coiled Circular Tubes," Chem. Eng. J., **84**(3), pp. 223–237.
[32] Kline, S. J., and McClintock, F. A., 1953, "Describing Uncertainties in Single-Sample Experiments," Mech. Eng., **75**(1), pp. 3–8.
[33] White, C. M., 1932, "Friction Factor and Its Relation to Heat Transfer," Trans. Inst. Chem. Eng., **18**, pp. 66–86.